

C.2



RESEARCH MEMORANDUM

FLUTTER INVESTIGATION AT LOW SPEED
OF A 40° SWEEPBACK WING WITH PYLON-MOUNTED STORES, TESTED
AS A SEMISPAN-CANTILEVER WING AND AS A FULL-SPAN WING ON
A TOWED AIRPLANE MODEL

By Albert P. Martina

CLASSIFICATION CHANGED

Langley Aeronautical Laboratory

UNCLASSIFIED

Langley Field, Va.

LIBRARY COPY

SEP 12 1956

NATIONAL ADVISORY COMMITTEE
FOR AERONAUTICS
LANGLEY FIELD, VIRGINIA

CLASSIFIED DOCUMENT

This material contains information affecting the National Defense of the United States within the meaning of the espionage laws, Title 18, U.S.C., Secs. 793 and 794, the transmission or revelation of which in any manner to an unauthorized person is prohibited by law.

NATIONAL ADVISORY COMMITTEE FOR AERONAUTICS

WASHINGTON
September 7, 1956

NACA RM L56F14a



NATIONAL ADVISORY COMMITTEE FOR AERONAUTICS

RESEARCH MEMORANDUM

FLUTTER INVESTIGATION AT LOW SPEED

OF A 40° SWEEPBACK WING WITH PYLON-MOUNTED STORES, TESTED
AS A SEMISPAN-CANTILEVER WING AND AS A FULL-SPAN WING ON

A TOWED AIRPLANE MODEL

By Albert P. Martina

SUMMARY

Wind-tunnel flutter investigations at Mach numbers up to 0.30 have been conducted on a 40° sweptback wing having pylon-mounted stores located at 73.5 percent of the semispan. The investigations were conducted on a semispan-cantilever wing with root fixed and with the full-span wing mounted on an autopilot-controlled model of a fighter-type airplane flown on the end of a towline. The store loadings were varied from 55 to 88 percent of the wing-panel weight, and the store pitch inertias were varied from 66 to 181 percent of the wing-panel pitch inertia. Most of the data were obtained with the store centers of gravity located at 15 percent of the local wing chord.

Flutter in the fixed-root cases was of the limited-amplitude, bending-torsion type with the torsion component predominant. The flutter speeds dropped sharply with increased store-to-wing inertia ratios. An increase in the store loadings from 66 to 88 percent of the wing weight increased the flutter speeds as much as 36 percent for a given store-to-wing inertia ratio.

Tunnel airspeed limitations prevented the attainment of flutter in the towed-model tests, although three configurations reached varying degrees of low damping behavior. Symmetrical bending-torsion response modes were indicated for one 66-percent loading case while two 88-percent loading cases exhibited the development of antisymmetrical bending-torsion modes. The marked differences between the fixed-root flutter velocities and the towed-model behavior indicated that the effects of body freedoms were quite large for certain loadings. For one 88-percent loading, the towed-model flutter velocity was at least 147 percent of the fixed-root velocity.

~~CONFIDENTIAL~~

The National Advisory Committee for Aeronautics recognizes the need for the development of wind-tunnel flutter-test techniques which allow body freedoms and which have possibilities of being used in the transonic regime. One such technique is the towed-airplane-model test technique in which all the degrees of freedom except longitudinal translation are provided and the stability and control is supplied by an autopilot.

Exploratory tests utilizing the towed-model technique were reported in reference 1 for an essentially rigid model having a flexible 40° swept-back wing that was fluttered at various speeds up to 260 feet per second by varying the mass parameters of the external stores. The results of the tests of reference 1 appeared promising enough to justify the continuation of the development of the technique, inasmuch as the electrical power failure which caused the nonflutter destruction of the towed model of reference 1 was easily remedied.

Accordingly, a second essentially rigid model with flexible wings was subsequently built with the capability of being tested in the Langley 16-foot transonic tunnel so that, among other things, autopilot response could be determined at speeds of the order of 600 feet per second. The general aerodynamic design of the second model was quite similar to that employed in reference 1 and utilized a wing that was somewhat stiffer to increase the wing flutter speed.

The present report presents the results of preliminary check-out tests that were made in the Langley 19-foot pressure tunnel up to a maximum velocity of the order of 350 feet per second. In order to develop wing flutter within the tunnel speed range, it was necessary to test heavier store loadings than those employed in the tests of reference 1. In essence, therefore, this report extends the investigation of reference 1 into a heavier store loading range. Store loadings varying from 55 to 88 percent of the wing panel weight were briefly investigated. Most of the data are from cantilever flutter tests. The results of several towed-model tests are also included. The tests were conducted at atmospheric pressure at Mach and Reynolds numbers ranging from 0.20 to 0.30 and 2.2 to 3.0×10^6 , respectively.

SYMBOLS

The model axes system was a mutually perpendicular system having its origin at the model center of gravity (located in the model plane of symmetry) with the X-axis parallel to the fuselage center line and the Y-axis normal to the plane of symmetry.

~~CONFIDENTIAL~~

EI	flexural rigidity of wing section, lb-in. ²
GJ	torsional rigidity of wing section, lb-in. ²
I_X, I_Y, I_Z	moment of inertia of model about respective model axes, lb-in. ²
$I_{Y,s}$	polar moment of inertia of external store about an axis parallel to Y-axis and which passes through point of intersection of spar axis and plane passing through store axis parallel to XZ-plane, lb-in. ²
$I_{Y,w}$	polar moment of inertia of wing panel about an axis which is parallel to Y-axis and which passes through panel center of gravity (see fig. 2(a)), lb-in. ²
I_α	polar moment of inertia of wing section about spar axis, lb-in. ² /in.
K_θ'	elevator-position control gearing ratio, δ_e/θ'
K_ϕ	roll-autopilot gearing ratio, δ_a/ϕ
K_ψ'	rudder-position control gearing ratio, δ_r/ψ'
$K_{\dot{\psi}}$	yaw-damper gear ratio, $\delta_r/\dot{\psi}$
M	Mach number
R	Reynolds number
V	velocity, fps
V_f	experimental flutter speed, fps
W	weight of model, lb
W_w	weight of wing panel, lb
W_s	weight of external store and pylon, lb
c	wing chord parallel to airstream, in.
c'	wing chord normal to spar axis, in.

\bar{c}	wing mean aerodynamic chord, in.
f	wing response frequency, cps
f_f	flutter frequency, cps
f_n	experimental frequency of vibration of wing in nth natural mode, cps
g	total damping coefficient, $\frac{1}{n\pi} \log_e \frac{\text{Amplitude at 0 cycles}}{\text{Amplitude at n cycles}}$
l	length of wing along spar axis, in.
l_s	length of external store, in.
w	weight of wing section of unit width, lb/in.
\bar{x}	location of model center of gravity measured from leading edge of mean aerodynamic chord, positive rearward, in.
\bar{x}_n	location of external-store center of gravity measured from nose of store, in.
\bar{x}_s	location of external-store center of gravity measured in streamwise plane from nose of wing section at spanwise location of store, positive rearward, in.
\bar{x}_O'	location of center of gravity of wing section from leading edge of section in a plane normal to spar axis, in.
y'	distance along spar axis from model center line, positive toward tip, in.
\bar{z}	vertical location of model center of gravity from fuselage reference line, positive upwards, in.
\bar{z}_s	vertical location of external-store center of gravity measured from spar axis parallel to Z-axis, positive upward, in.
δ_a	total (left plus right) aileron deflection normal to aileron hinge axis, positive to produce positive roll, radians
δ_e	elevator deflection normal to elevator hinge axis, positive trailing edge down, radians

δ_r	rudder deflection normal to rudder hinge axis, positive trailing edge left, radians
θ'	angle between a plane parallel to XY-plane and a plane normal to XZ-plane and containing the tow rod, radians
ρ_f	density of air at flutter, slugs/cu ft
ϕ	angle of roll, radians
ψ'	angle between XZ-plane and a plane normal to XY-plane and containing the tow rod, radians
$\dot{\psi}$	yawing angular velocity, radians/sec
ω_2	angular frequency of vibration in second mode, $2\pi f_2$, radians/sec
$\frac{2V_f}{\omega_2 c}$	flutter speed coefficient, referred to wing mean aerodynamic chord

MODEL

The model used in this investigation was constructed in a manner which was generally similar to that used in reference 1. The model description in the present paper treats the wings in some detail and shows improvements and differences of the present model over that of reference 1. The model, as in reference 1, was representative of a fighter-type airplane although there were some differences in the overall mass characteristics.

Pertinent dimensions of the wing as mounted on the towed model are given in figure 1. The model and store mass characteristics are given in tables I, II, and III. The various model configurations are designated by a system of numbers which describe the principal mass parameters of the stores as described in table I.

The wing was swept back 40° at the quarter-chord line, had an aspect ratio of 3.45, a taper ratio of 0.579, and embodied a negative dihedral of 3.5° . The airfoils were of NACA 64A010 sections normal to the quarter-chord and had a 7.8-percent streamwise thickness-chord ratio. Each wing panel consisted of an aluminum-alloy spar to which were attached 12 balsa segments or "pods" which formed the wing surfaces as shown in figure 2.

The wing spar axis had 37.25° sweepback and intersected the theoretical root and tip chords at 42 and 38 percent of the respective chords. The gaps between pods were aerodynamically sealed by covering the entire wing panel with 0.008-inch rubber sheet bonded to the pods with rubber cement. The structural properties of the covered-wing panels assembled with ailerons are given in figure 3. The bending and torsional rigidities were determined from measurements of the spanwise slope and twist distributions of the respective deflection curves obtained from the application of known moments to the panels. The drag stiffness on the other hand was calculated by the use of simple beam theory.

All the pods were ballasted with lead shot bonded together with a plastic binder in cavities drilled within the pods. The ballasting masses were constructed in this manner so that, in the event of any wing failure, small, disintegrable masses would be introduced into the tunnel circuit and reduce the likelihood of severe tunnel damage. The spanwise variations of the wing mass parameters are given in figure 4. The mass parameters of the pods were adjusted experimentally to match closely the design values. The section moments of inertia were obtained by experimentally determining the moment of inertia of each of the ballasted rubber-covered pods on a bifilar pendulum, adding in the calculated spar contributions, and dividing by the pod widths. The overall mass properties of the entire wing are given in figure 2. An indication of the dynamic similarity of the left and right wing panels without stores can be obtained from the following table of cantilever frequencies.

Wing panel	f ₁ first bending	f ₂ first torsion	f ₃ second bending
Left	12.62	45.3	50.0
Right	12.70	45.8	52.0

The nodal patterns given in figure 5 were similar within the accuracy of measurement.

The ailerons were mass-balanced and aerodynamically balanced and had hinge lines at 0.25 normal chord. The inner ends of the aileron torque tubes (see fig. 2) were fixed to self-aligning ball bearings which were mounted inside either the fuselage or the reflection plane. The aileron restraint in the fixed-root tests was sufficiently rigid to prevent aileron rotation, whereas the aileron was restrained by the roll gyro in the towed-model tests. The universal joints at the inboard ends of the ailerons (see fig. 2) combined with the self-aligning bearings at the hinge brackets and the slip fits between the aileron hinge pins and the inner races of the

hinge-bracket bearings allowed the ailerons enough freedom to prevent bind for combined bending and twist deflections at the tip of 1 inch and 6° , respectively. The vibration characteristics of the wing panels in the fixed-root and towed-model tests are given in tables IV and V. The towed-model frequencies were determined with the model hung vertically from the towline with excitation applied at various points depending on the mode being sought. The lowest wing fore and aft frequencies were obtained for the 88-percent loading conditions and were approximately 19 cps, well outside the flutter range. All other model components were made as rigid as weight limitations would allow.

In general, the autopilot system of the towed model was identical to that of reference 1. A decided improvement in this model over that of reference 1 was the ability to change the proportional autopilot linkage ratios in flight, so that the towed model could be flown with a minimum of large oscillations at all speeds.

The external stores were mounted on rigid underslung pylons at 73.5-percent semispan. The store moments of inertia were varied by changing the positions of bismuth-tin weights in the forebody and afterbody. The store centers of gravity were determined by resting the store successively on two sets of knife edges affixed to the store and plotting the intersection of vertical lines passing through the respective knife edges on a store-attached grid by means of an engineer's transit. The store moments of inertia were determined by oscillating a store as a compound pendulum on a knife edge attached to the pylon mounting pad. An automatic electronic timer was used to time the oscillations.

The lowest pylon frequencies were naturally obtained with the heaviest or the 88-15-170 store loading. With the pylon clamped rigidly, the yaw frequency was approximately 25 cps, and the pitch frequency was approximately 44 cps. The side bending frequency was quite high and could not be excited with the available equipment. These pylon frequencies were only slightly lower with the store mounted on the wing for this loading condition; thus it is seen that the pylon frequencies were well outside the flutter frequency range. The zero airspeed damping coefficients of the wing panels as determined from decay records ranged from 0.02 to 0.03 in the first two vibration modes for all of the fixed-root configurations.

Larger capacity flutter dampers of the type employed in reference 1 were mounted in the stores for the towed-model tests for protection against divergent flutter.

INSTRUMENTATION AND APPARATUS

The setup of a model wing panel for the fixed-root tests is shown in figure 6 and was identical to that employed in reference 1. The towed-model setup shown in figure 7 differed from that of reference 1 only in that no snubbing wire was used. Electric-pen two-channel recording oscillographs operating at low speed and located at the flutter observer's station were added for these tests. They were placed in the observer's field of view so that he could maintain visual contact with the model. The observer monitored the innermost (0.23 semispan) bending and torsion strain-gage outputs.

TEST PROCEDURE

The tests were conducted in the Langley 19-foot pressure tunnel at atmospheric pressure. The resulting Mach and Reynolds number variation with airspeed are presented in figure 8 for the test range. The test procedure, in general, was identical to that employed in reference 1 in that, as the wing damping appeared to decrease, airspeed changes were made in progressively smaller increments. Inasmuch as some of the heavy, high inertia configurations in the fixed-root tests experienced a wide speed range of low damping, and only small increases in the amplitudes of motion at flutter, the electric-pen recording oscillographs proved to be a very dependable means of flutter detection. In no case was the model damaged as a result of flutter.

No corrections to the fixed-root flutter speeds were made for the boundary layer on the reflection plane. The small thickness of the boundary layer relative to the model span resulted in average velocities in the region occupied by the model which were within 1 percent of the true velocity as explained in reference 1.

It was not possible to evaluate the effects on the observed flutter speeds of probable differences in turbulence and aileron restraint between the fixed-root and the towed-model tests.

RESULTS AND DISCUSSION

Fixed-Root Tests

The flutter characteristics are presented in table IV and in figure 9. Flutter in all cases was of the limited-amplitude bending-torsion type with the torsion component predominant. The flutter frequencies in most cases

were quite near the zero-speed torsion frequencies. Tip amplitudes reached during flutter ranged from $1/4$ to $1/2$ inch in bending and 1° to 2° in torsion.

Inasmuch as the bending strain gages at the 0.23-semispan station indicated either no oscillations or oscillations of very low amplitude at the flutter speed, the tunnel velocities were carried somewhat beyond the flutter speeds in order to explore this observed behavior. It was found that, at the 0.23-semispan station steady periodic oscillations in torsion at the flutter frequency usually set in at the flutter speed, although in some cases these torsional oscillations did not set in until $1.07V_f$. The bending gage outputs indicated occasional flutter bursts of approximately 10 cycles duration. The periodicity of the bursts increased with increased tunnel speed until a constant amplitude was indicated at speeds ranging from $1.12V_f$ to $1.22V_f$. Noticeable increases in the oscillation amplitudes occurred concurrently. Frequencies changed slightly and phase angles appeared to remain constant during this period. Portions of oscillograms of a typical case are shown in figure 10 for velocities of $1.00V_f$ and $1.14V_f$.

The flutter-speed variations with store mass parameters are presented in figure 9. In general, the flutter speeds were greatly influenced by changes in the store-wing pitch inertia ratios, and decreased linearly with increasing store-wing inertia ratios. Moving the store centers of gravity forward from 15 percent to 11 percent of the chord or rearward to 19 percent of the chord had negligible effects on the flutter speeds. A similar effect was noted in reference 1 for a 56-percent loading. Increasing the store loadings from 66 to 88 percent raised the flutter speeds about 70 feet per second which resulted in increases in the flutter speeds of from 23 to 36 percent over the store-wing inertia range covered in the tests.

Towed-Model Tests

Prior to the towed-model tests, tunnel turbulence-damping screens had been installed for other tests. As a consequence, the tunnel maximum air-speed for the towed-model tests was nearly 15 percent lower than for the fixed-root tests which had been made before the screen installation. As a result of this lowered tunnel maximum speed it was felt that only four of the fixed-root test configurations might flutter on the towed model within the speed range available.

The four configurations were each tested to the maximum tunnel speed. None of the configurations fluttered although three of the configurations reached varying degrees of low damping behavior. The 88-15-104 configuration appeared to have come nearest to flutter. The damping at the maximum

speed for this case was only slightly positive, about one-third of the wing structural damping, and decays of the order of 25 to 40 cycles duration were recorded. A summary of the behavior observed in the four towed-model tests is presented below in the estimated order of decreasing proximity to flutter:

Configuration	V_{max} , fps	ξ_{min}	f, cps	Response mode
88-15-104	301.0	<0.01	11.05	Antisymmetrical
88-15-170	317.0	.03	8.55	Antisymmetrical
66-15-127	319.7	.06	10.82	Symmetrical ^a
57-15-66	315.4	High	^b 12 to 13	-----

^aPrincipal response; occasionally asymmetrical with bending symmetrical and left torsion as much as $\pm 50^\circ$ out of phase with right torsion

^bAmplitudes insufficient to determine response frequency with any certainty

Some remarks concerning the towed-model behavior particularly with regards to tunnel turbulence, and the determination of the values ξ_{min} are given in the appendix.

The towed-model test results are presented in figure 11 so that some idea of the trends of the towed-model flutter boundaries may be indicated. The fixed-root results have been superposed for reference purposes.

The differences between the fixed-root boundaries and the towed-model results were quite large for certain loadings. For the 66-percent store loading where a symmetrical mode was indicated it appeared that the towed-model flutter boundary at this point was at least 38 percent above the fixed-root boundary. For the 88-percent store loadings the towed-model flutter boundary was not less than 88 percent of the fixed-root flutter boundary at the lowest store-wing inertia ratio and, at the highest wing-store inertia ratio, was more than 147 percent of the fixed-root flutter speed. The cross-hatched trend was drawn in from considerations of the static frequency variations for these store loadings. The development of antisymmetric modes was indicated.

The higher flutter speed of the towed-model over the corresponding fixed-root case for the 66-percent loading when considered with the results of reference 1 for 33- and 56-percent store loadings, appeared to be nearly proportional to the increases in the store loadings. The increasing effects of body freedoms for the heavier store loadings together with the transition from symmetric to antisymmetric modes as the store loadings were increased from 66 to 88 percent of the wing-panel weight illustrates the importance of body freedom simulation. The importance of allowing as many body freedoms as practicable has also been demonstrated in reference 2 for a model having a greater number of structural flexibilities.

SUMMARY OF RESULTS

Low-speed wind-tunnel flutter investigations of a 40° sweptback wing equipped with pylon-mounted external stores having various loadings and tested as a semispan-cantilever wing with root fixed and as a wing on an autopilot-controlled towed airplane model indicated the following results:

1. Flutter in the fixed-root cases was of the limited-amplitude, bending-torsion type with the torsion component predominant.
2. The fixed-root flutter speeds decreased sharply with increased store-wing inertia ratios. The fixed-root flutter speeds increased as much as 36 percent with increased store loadings for a given store-to-wing inertia ratio. No changes in the flutter speeds resulted for small center-of-gravity variations in one case.
3. No flutter was encountered in the towed-model tests due to tunnel airspeed limitations, although three configurations reached varying degrees of low damping behavior. Bending-torsion response modes were exhibited, symmetrical in a 66-percent loading case and antisymmetrical in two 88-percent loading cases.
4. The marked difference between the trends of the towed-model and the fixed-root test results indicated that the effects of body freedoms were quite large for certain store loadings. For one 88-percent loading the towed-model flutter velocity was at least 147 percent of the fixed-root velocity. The effects of body freedoms were greater than the effects found in NACA Research Memorandum L54K17. The large magnitudes of the body freedom effects plus the changes from symmetric to antisymmetric modes between

the 66- and 88-percent loading cases reiterates the need already demonstrated for adequate body-freedom and aerodynamic simulation in cases of this kind.

Langley Aeronautical Laboratory,
National Advisory Committee for Aeronautics,
Langley Field, Va., June 1, 1956.

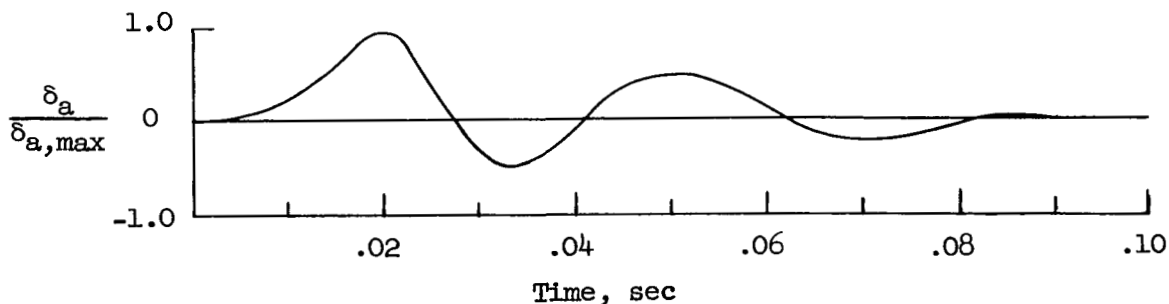
APPENDIX

MECHANISM OF EXCITATION OF THE TOWED-MODEL WING

PRODUCED BY TUNNEL TURBULENCE

Wind-tunnel turbulence produced wing excitation both directly and indirectly. The direct excitation from tunnel turbulence was of very low level and gave indications of the sense of the wing response modes. The wing excitation which resulted indirectly from tunnel turbulence was produced by the rapid antisymmetric deflection of the ailerons. The aileron excitation was random and appeared to depend mostly on the rate of change of tunnel airspeed as discussed later.

The mechanism of the aileron excitation can best be explained by considering the type of roll autopilot employed in the towed-model tests. The roll autopilot consisted of an electrically driven gyro oriented to furnish a reference in roll. The gyro was directly linked to the aileron so that the aileron deflections were proportional to the angle of bank of the towed model. The gyro was centered by a fast-acting torque motor which was energized by the closing of a centering contact on the gimbal of the gyro with either of two fixed-centering contacts. Whenever the angle of bank of the towed-model was large enough to cause the hinge moments from the ailerons to force the roll gyro to precess to the point where the centering contacts would close, then the fast-acting torque motor would apply a counter-torque to recenter the gyro gimbal between the contacts. Since the centering contacts of necessity were required to have a finite gap, the recentering of the roll gyro by the torque motor produced small, rapid antisymmetric deflections of the ailerons or pulse as shown by the following deflection time history where δ_a is the deflection of one aileron:



The value of $\delta_{a,max}$ was of the order of 2° . The aileron deflection frequencies during such a pulse recentering were essentially constant and ranged from 2 to 3 times the wing response frequencies.

~~CONFIDENTIAL~~

As previously stated, the occurrence of the aileron pulses depended mainly on the rate of change of tunnel airspeed. When tunnel airspeed was nearly constant, tunnel turbulence was at a minimum and the towed-model rolling oscillations were of small amplitude. Under these circumstances the aileron pulses occurred at the lowest rates. On the other hand when the tunnel airspeed was being changed, tunnel turbulence was at a maximum and the towed-model rolling oscillations tended to increase in amplitude. The aileron deflections consequently were larger and more frequent pulses were experienced, often having rates as high as five times per second. Aileron pulses occurring at these latter rates could sustain the model wing in an apparent state of flutter not unlike servo-coupled flutter if properly phased with the wing motions. The wing oscillations, of course, died out as a result of the decreased airstream turbulence accompanying the reestablishment of constant tunnel airspeed.

In the present tests only those periods of nearly constant tunnel airspeed were of concern. A portion of an oscillogram taken during such a period and following an aileron pulse is shown in figure 12. A single aileron pulse was not capable of producing the amplitudes of initial wing motions such as those shown in figure 12. A pulse was of sufficient strength, however, to amplify significantly or to stop wing motions depending on the phase relationship of the aileron pulse to the wing motions. Thus when excitation resulted, the aileron pulse provided a clear and definite reckoning point from which to assess the damping. The minimum values of the damping coefficient previously tabulated were determined from the wing decays following such aileron pulses.

In addition, even though the aileron excitation was antisymmetrical, it had but small effects on the symmetric response tendencies. The records for the behavior of the 66-15-127 configuration indicated that the discernible effects of a pulse disappeared rather quickly and the wing motions reverted to symmetrical. The few instances where a phase angle between the left and right wing torsion signals appeared were believed to be due to the phase relations of the pulse to the wing motions.

REFERENCES

1. Martina, Albert P., and Young, George E.: Results of Initial Wind-Tunnel Flutter Experiments at Low Speed With a Towed Airplane Model Having a 40° Sweptback Wing of Aspect Ratio 3.62 Equipped With Pylon-Mounted Stores. NACA RM L54K17, 1955.
2. Kinnaman, E. Berkeley: Flutter Analysis of Complex Airplanes by Experimental Methods. Jour. Aero. Sci., vol. 19, no. 9, Sept. 1952, pp. 577-584.

TABLE I.- EXTERNAL-STORE MASS PARAMETERS
FOR FIXED-ROOT TESTS

[All values presented for right-hand store]

Configuration (a)	W_s , lb	W_s/W_w	$I_{Y,s}$, lb-in. ²	$I_{Y,s}/I_{Y,w}$	\bar{x}_s/c	\bar{z}_s/c	\bar{x}_n/l_s
55-15-94	7.58	0.547	975	0.94	0.153	-0.247	0.464
66-15-106	9.11	.658	1,097	1.06	.152	-.248	.464
66-15-120	9.11	.658	1,238	1.20	.153	-.248	.464
66-15-136	9.11	.658	1,400	1.36	.153	-.248	.464
66-11-123	9.11	.658	1,268	1.23	.106	-.254	.440
66-19-123	9.11	.658	1,275	1.23	.194	-.240	.485
78-15-181	10.81	.781	1,867	1.81	.150	-.249	.462
88-15-111	12.18	.879	1,147	1.11	.152	-.250	.463
88-15-144	12.18	.879	1,492	1.44	.152	-.250	.463
88-15-163	12.14	.877	1,682	1.63	.151	-.250	.463

^aStore configurations are designated as follows: The first number represents W_s/W_w , the second number represents \bar{x}_s/c , and the third number represents $I_{Y,s}/I_{Y,w}$.

TABLE II.- EXTERNAL-STORE MASS PARAMETERS
FOR TOWED-MODEL TESTS

Configuration	Store	W_s , lb	W_s/W_w	$I_{Y,s}$, lb-in. ²	$I_{Y,s}/I_{Y,w}$	\bar{x}_s/c	\bar{z}_s/c	\bar{x}_n/l_s
57-15-66	Left	7.90	0.570	679	0.657	0.152	0.253	0.459
	Right	7.91	.571	680	.658	.152	.253	.463
66-15-127	Left	9.21	.665	1,312	1.270	.153	.253	.460
	Right	9.16	.661	1,316	1.274	.152	.255	.463
88-15-104	Left	12.22	.882	1,072	1.038	.153	.256	.459
	Right	12.25	.885	1,075	1.041	.153	.258	.463
88-15-170	Left	12.22	.882	1,760	1.704	.152	.256	.459
	Right	12.25	.885	1,764	1.708	.154	.257	.465

TABLE III.- TOWED-MODEL MASS PARAMETERS

Store configuration	W, lb	\bar{x}/\bar{c}	\bar{z}/\bar{c}	$I_X,$ lb-in. ²	I_Y	I_Z
88-15-104	104.9	0.292	-0.122	25,390	22,700	46,340
88-15-170	104.9	.292	-.122	25,390	24,080	47,720
66-15-127	98.8	.276	-.105	21,490	23,040	42,810
57-15-66	96.3	.268	-.098	19,860	21,690	39,840
Without stores	80.4	.212	-.044	9,640	19,680	27,910

TABLE IV.- FLUTTER CHARACTERISTICS OF RIGHT MODEL WING
 PANEL FROM FIXED-ROOT TESTS

Store configuration	Flutter characteristics				Wing characteristics (zero speed)		
	V_f , fps	f_f , cps	$\frac{2V_f}{\omega_2 c}$	ρ_f , slugs/cu ft	f_1 , cps (a)	f_2 , cps (b)	f_1/f_2
55-15-94	298.0	11.20	5.04	0.002484	8.93	11.24	0.792
66-15-106	291.5	10.61	5.11	.002315	8.37	10.83	.773
66-15-120	247.5	9.78	4.47	.002342	8.31	10.52	.790
66-15-136	208.5	9.75	3.96	.002379	8.18	10.00	.818
66-11-123	236.0	10.19	4.33	.002489	8.15	10.35	.780
66-19-123	239.0	10.22	4.37	.002474	8.48	10.38	.816
78-15-181	176.5	8.54	3.93	.002447	7.27	8.57	.848
88-15-111	337.0	10.20	6.27	.002258	7.72	10.67	.723
88-15-144	269.3	8.84	5.79	.002334	7.64	9.49	.805
88-15-163	215.0	8.85	4.62	.002382	7.63	9.00	.850

^aPredominantly first bending mode.

^bPredominantly first torsion mode.

TABLE V.- TOWED-MODEL TEST CHARACTERISTICS

Store configuration	Test behavior			Wing characteristics (zero speed)						Autopilot parameters			
				Symmetric			Antisymmetric			Pitch	Yaw		Roll
	V_{max} , fps	f, cps	Response mode	f_1 , fps (a)	f_2 , fps (b)	f_1/f_2	f_1 , fps	f_2 , fps	f_1/f_2	K_{θ} '	K_{ψ} '	$K_{\dot{\psi}}$	K_{ϕ}
88-15-104	^c 301.0	11.04	Antisymmetrical	10.64	10.82	0.93	11.16	11.16	1.00	1.80	1.00	0.17	7.54
88-15-170	^c 317.0	8.55	Antisymmetrical	10.25	8.96	1.14	8.75	11.83	.75	1.80	1.00	.36	7.54
66-15-127	^c 319.7	10.82	Symmetrical	10.93	10.45	1.05	-----	-----	-----	1.70	1.00	.21	7.54
57-15-66	315.4	12.13	-----	11.25	15.14	.74	-----	-----	-----	1.25	1.00	.40	6.80

^aPredominantly bending.^bPredominantly torsion.^cLow damping behavior.

CONFIDENTIAL

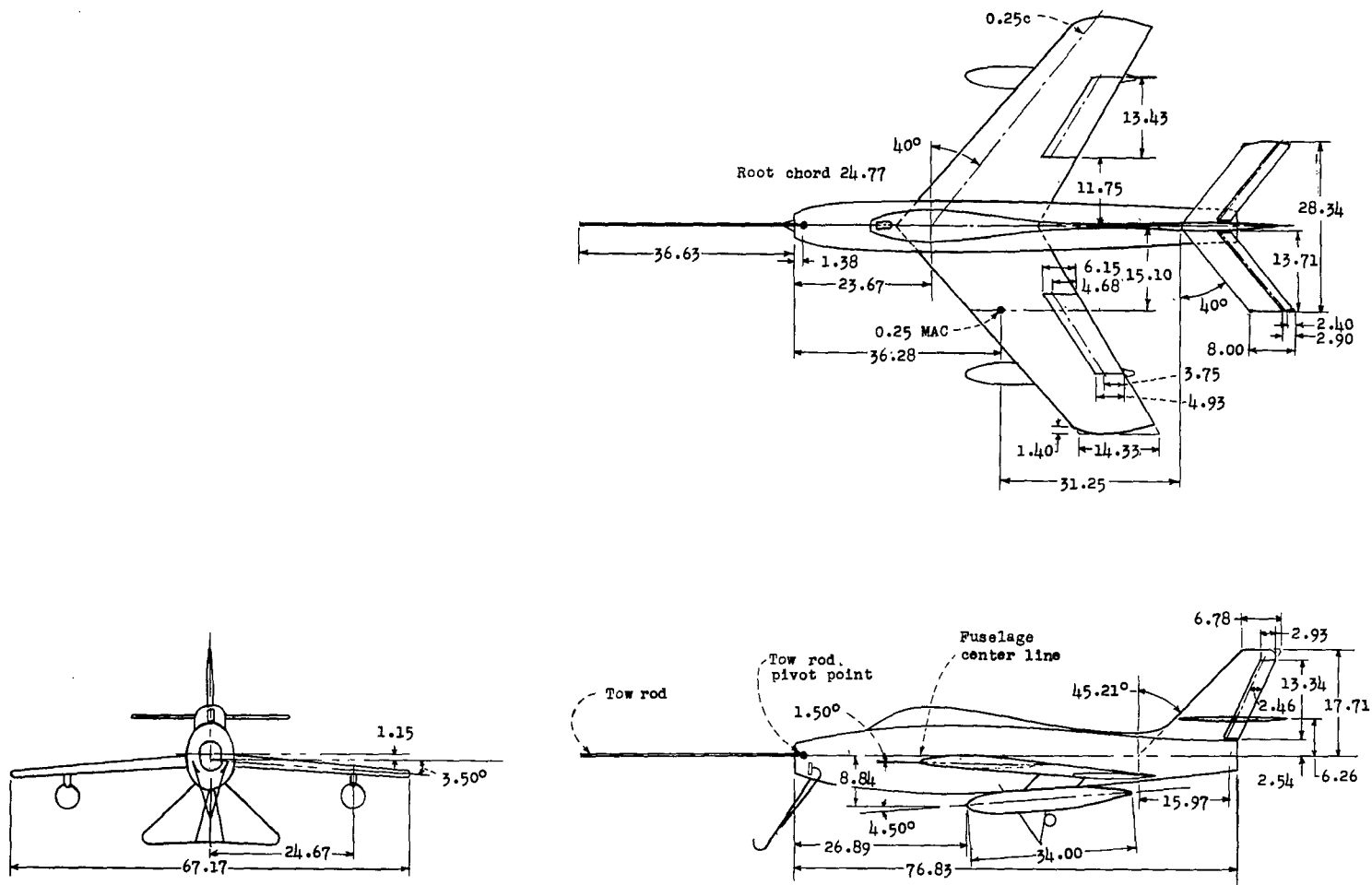
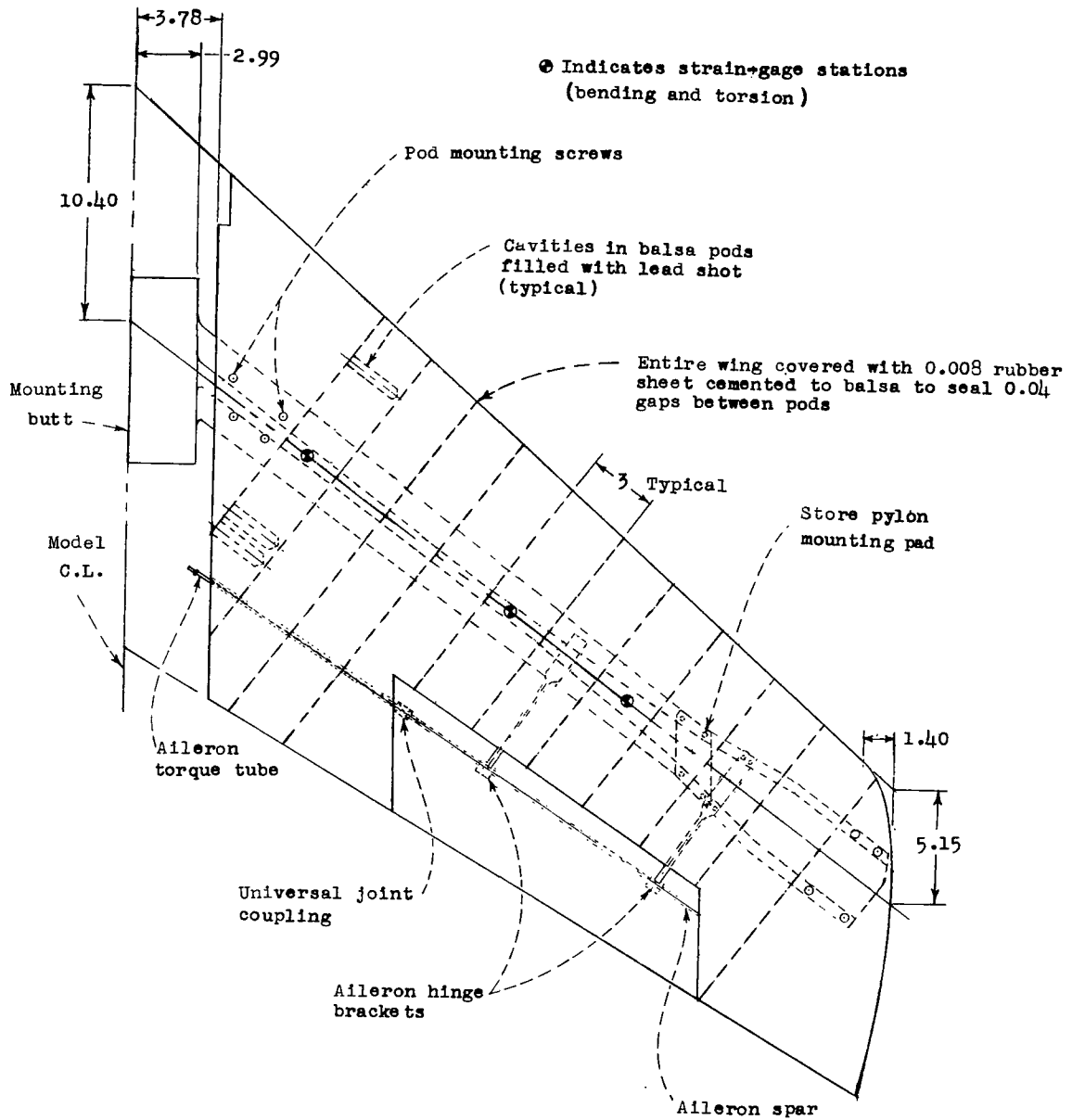
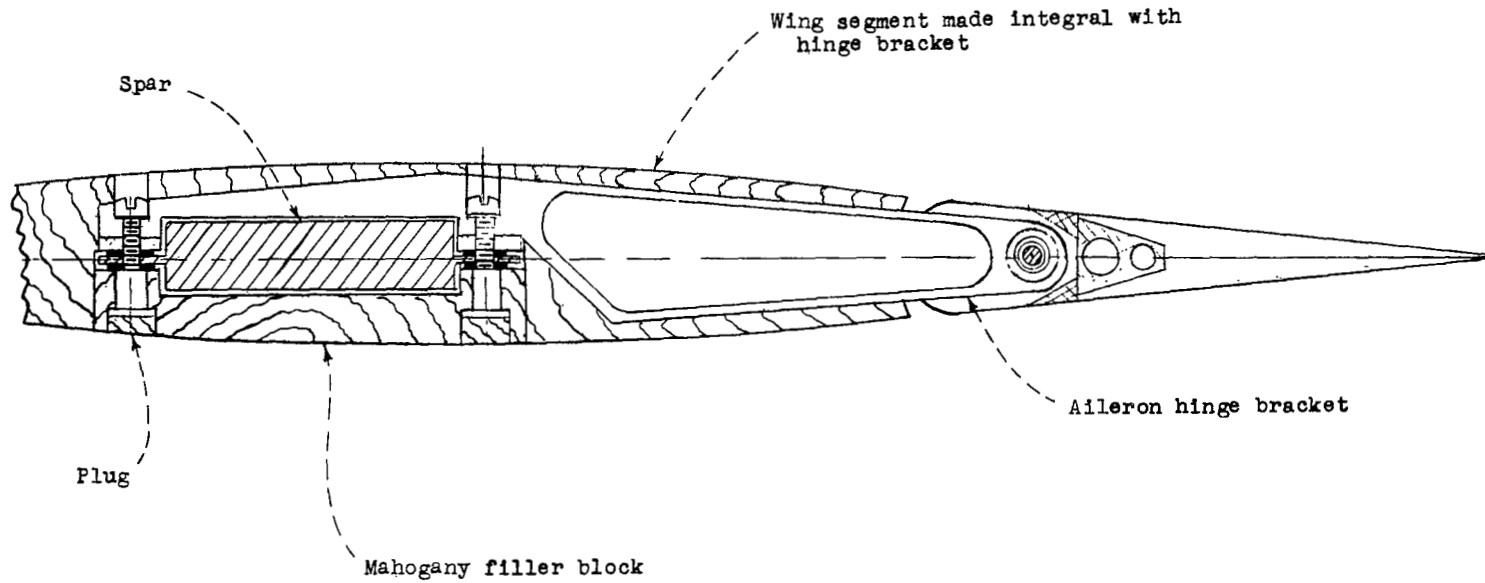


Figure 1.- Principal dimensions of the model. Wing area, 9.03 square feet; taper ratio, 0.579; mean aerodynamic chord, 20.08 inches. All dimensions are in inches unless otherwise noted.



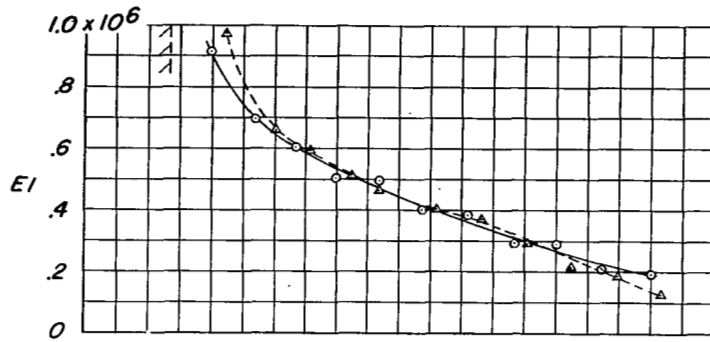
(a) Overall assembly. Weight 13.85 pounds neglecting mounting butt; longitudinal center of gravity 22.87 inches aft of nose of root chord; $I_{Y,W} = 1,033 \text{ lb-in.}^2$. All dimensions in inches.

Figure 2.- Construction details of model wing panels.

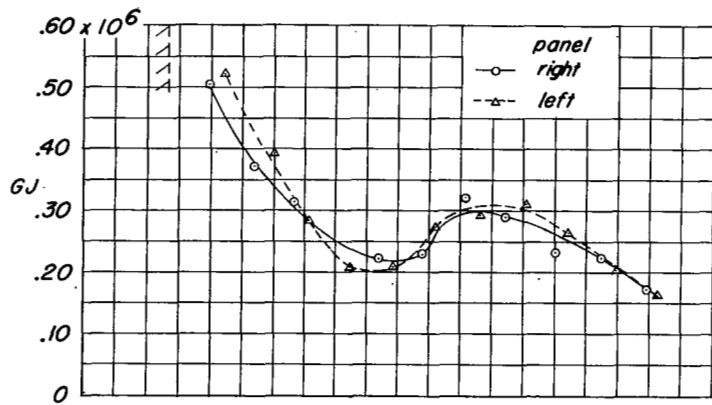


(b) Section through outboard aileron-hinge bracket showing attachment to spar.

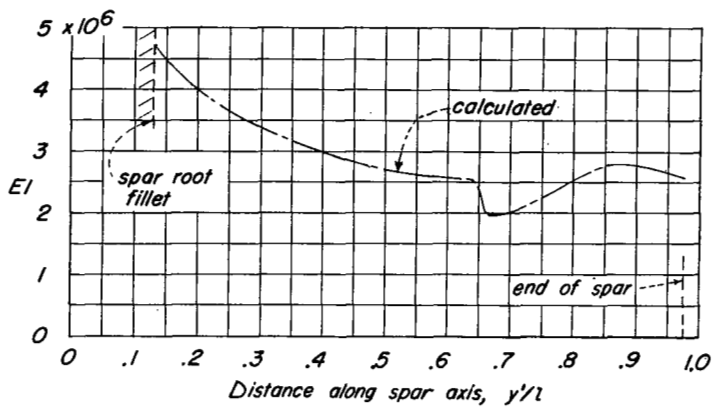
Figure 2.- Concluded.



(a) Bending rigidity.

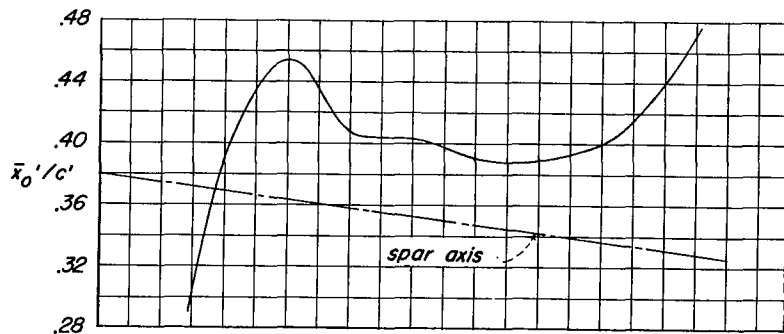


(b) Torsional rigidity.

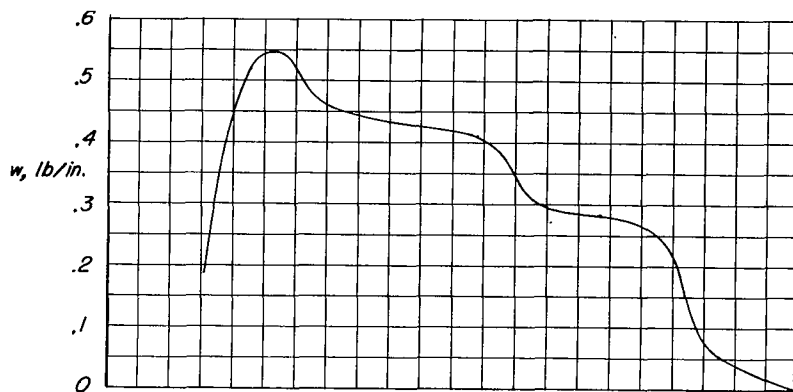


(c) Drag stiffness.

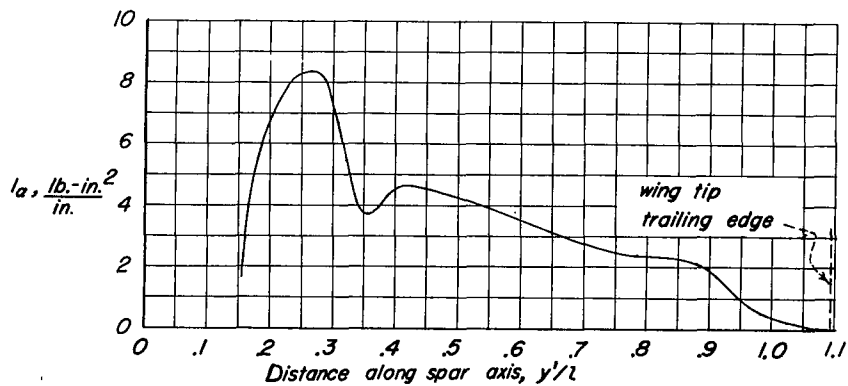
Figure 3.- Structural characteristics of the model wing panels.



(a) Section centers of gravity.



(b) Weight distribution.



(c) Section weight moments of inertia about spar axis.

Figure 4.- Mass parameters of model wing panels.

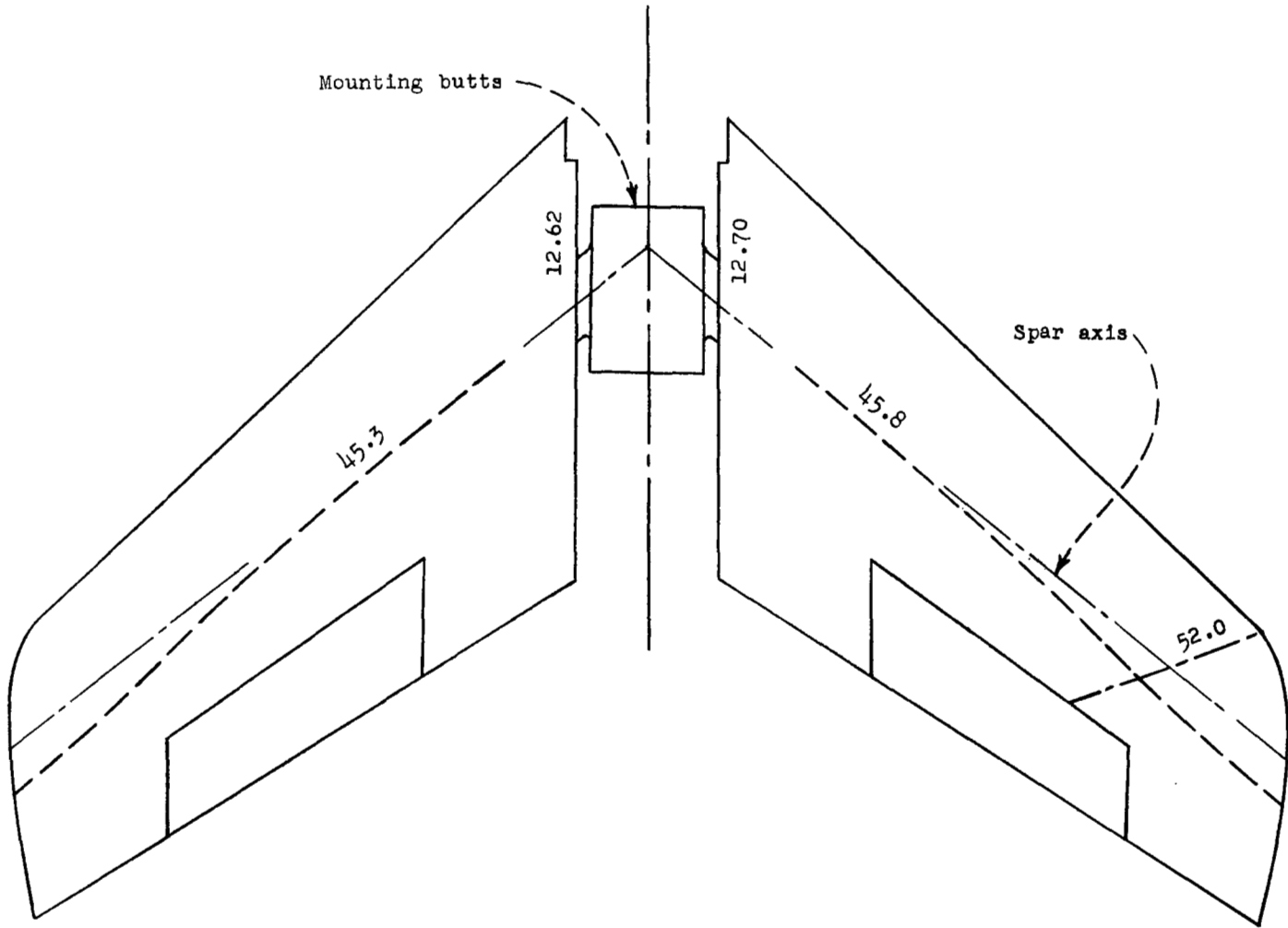


Figure 5.- Nodal line patterns for wing panels without stores and with the mounting butts fixed. Nodal line on left panel for 50 cps was not determined.

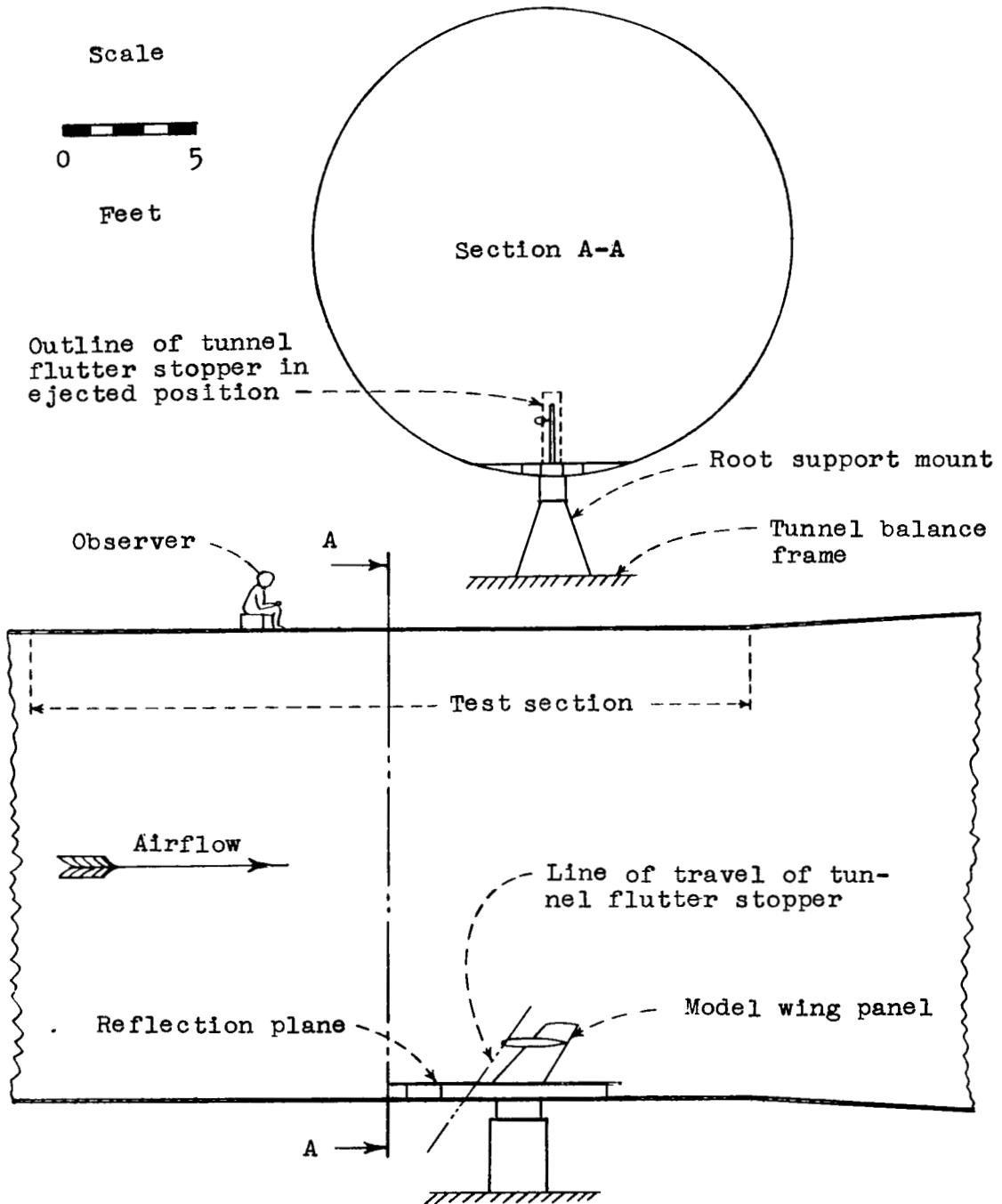


Figure 6.- Fixed-root flutter-test setup in the Langley 19-foot pressure tunnel.

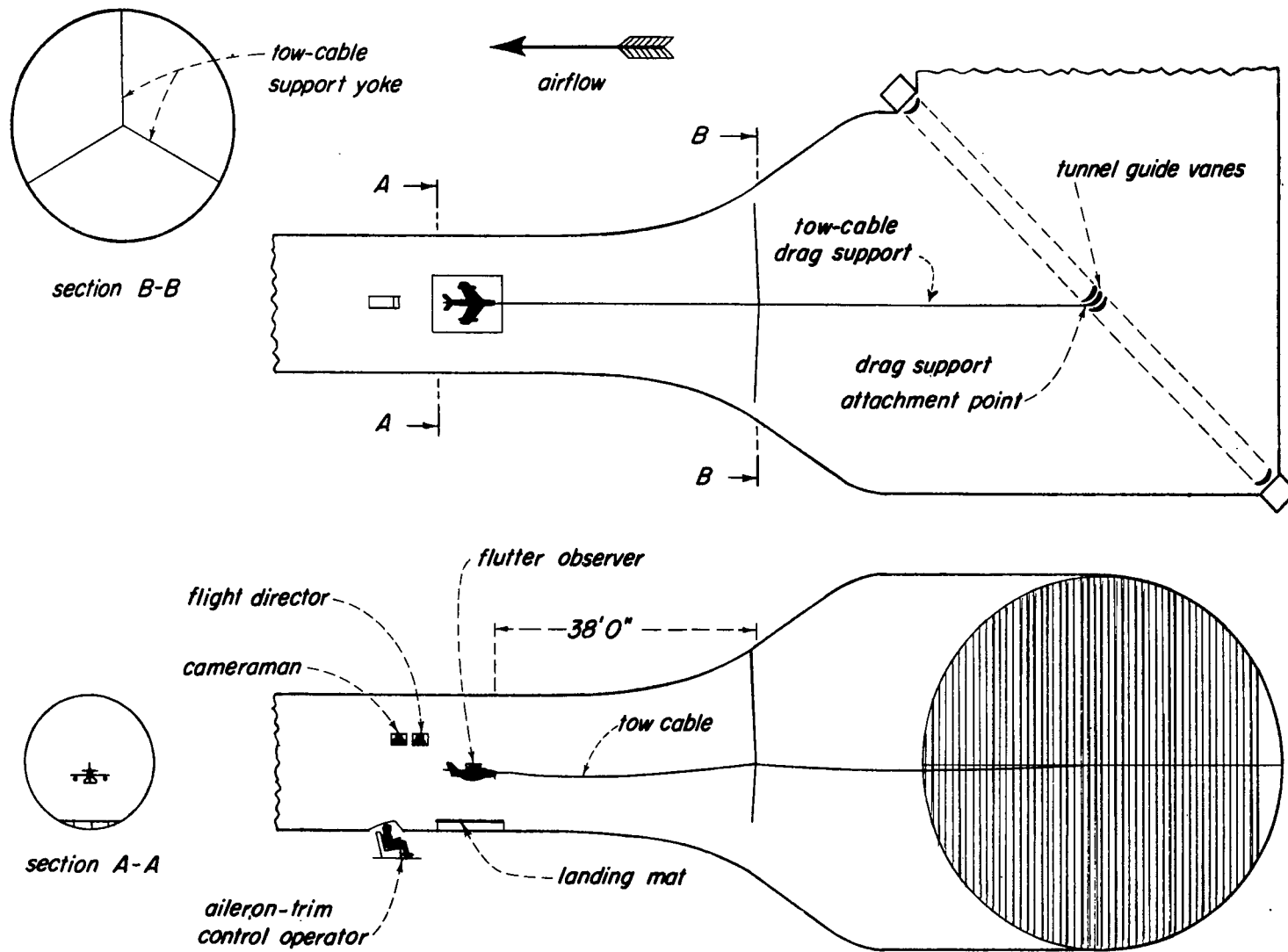


Figure 7.- Langley 19-foot pressure tunnel towed-model test arrangement.

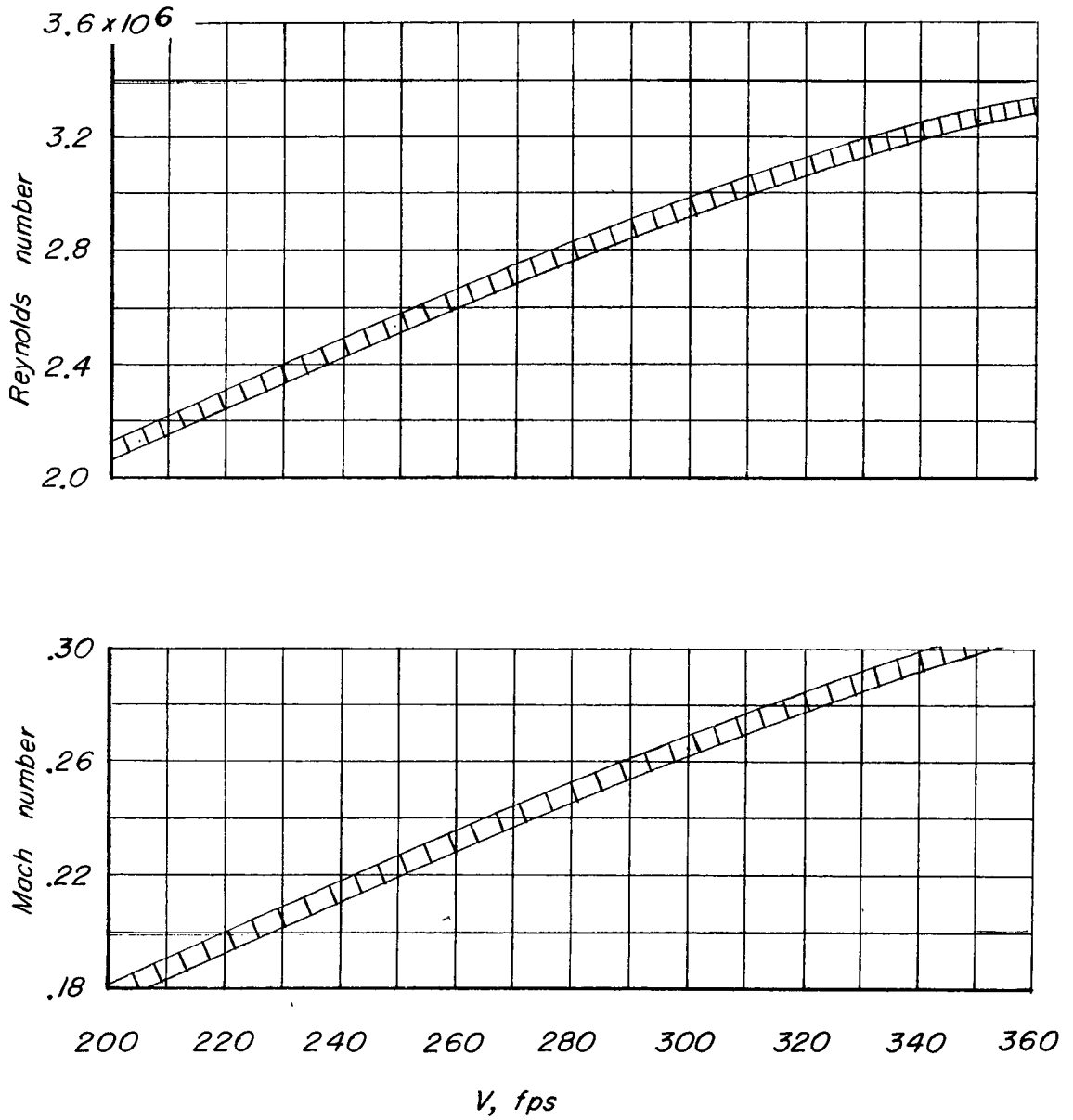


Figure 8.- Reynolds and Mach number variations of tests.

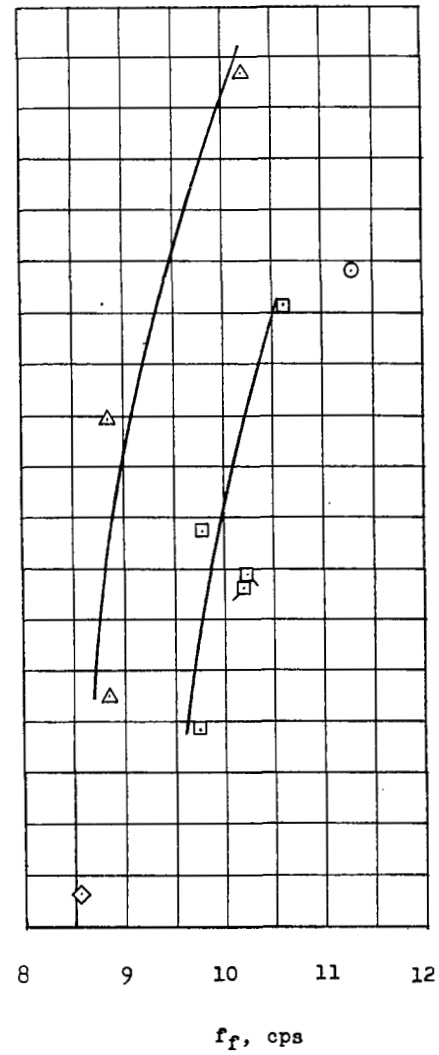
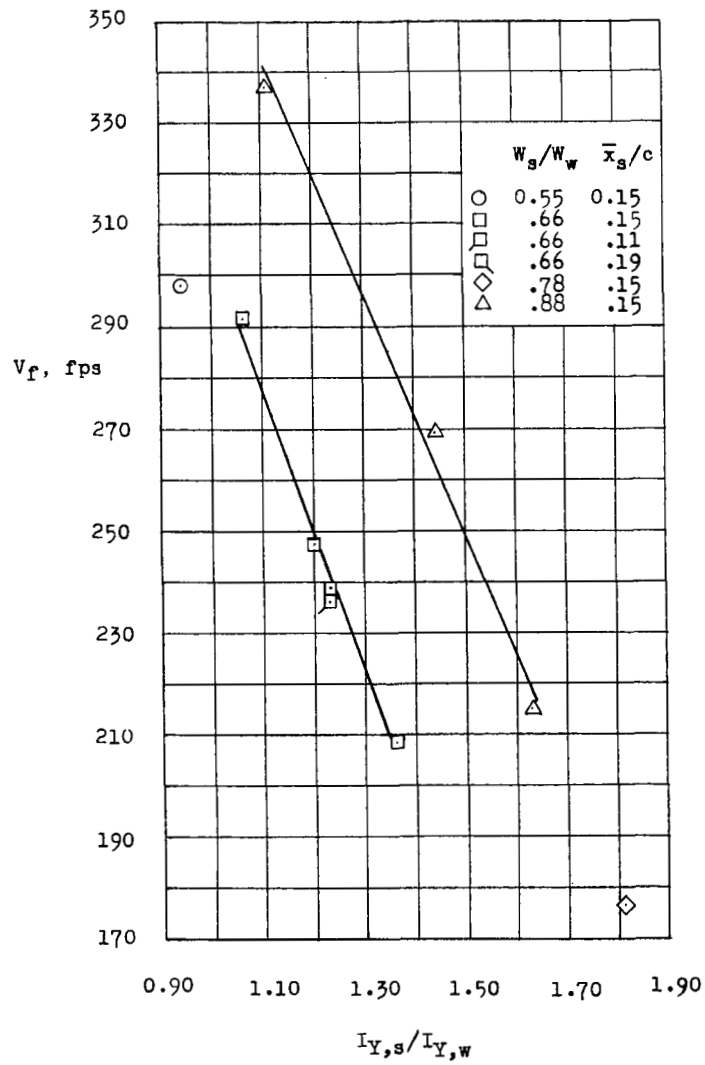
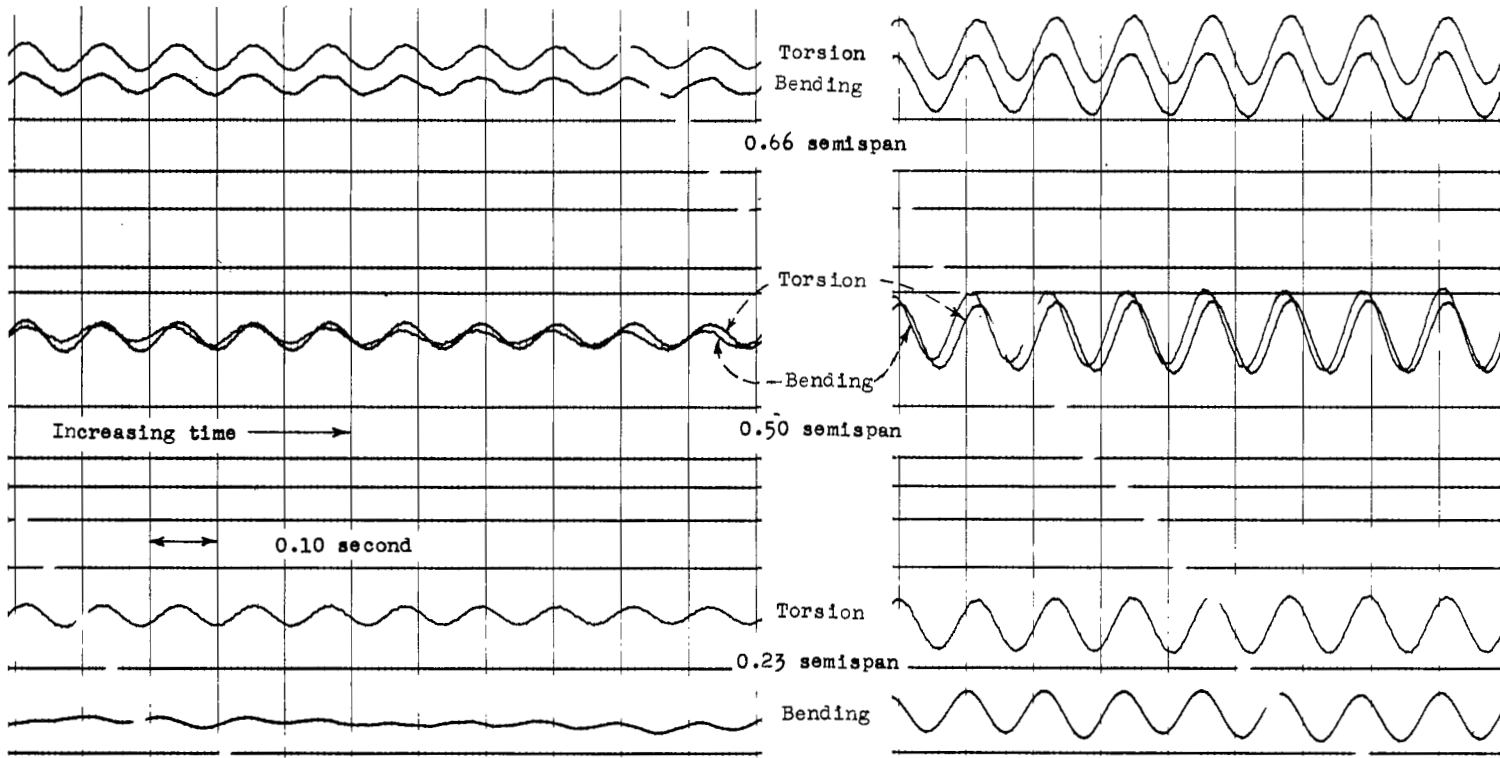


Figure 9.- Flutter characteristics of right-hand model-wing panel and store tested with root fixed.



(a) $1.00V_f$.

(b) $1.14V_f$.

Figure 10.- Portions of typical oscillograms taken during fixed-root tests showing post flutter behavior at the 0.23-semispan station. Directions of downward bending and torsion producing increased angles of attack are from bottom to top of figure.

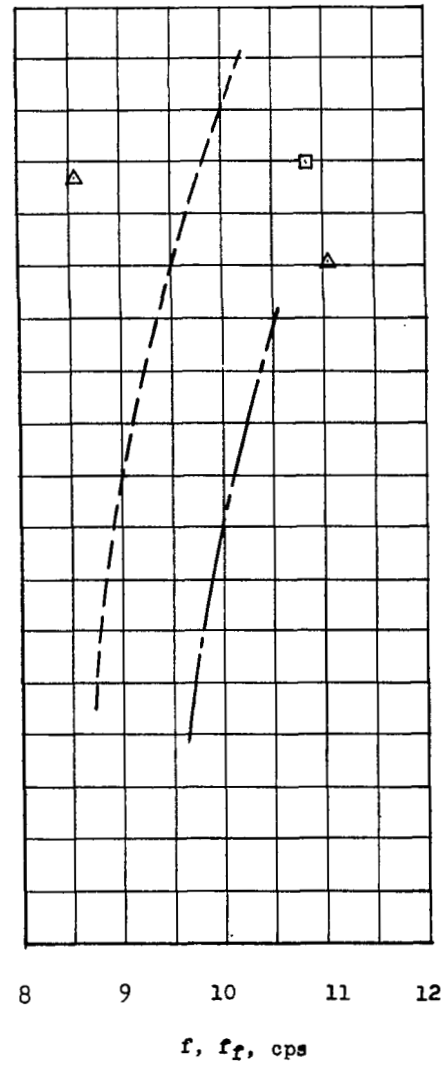
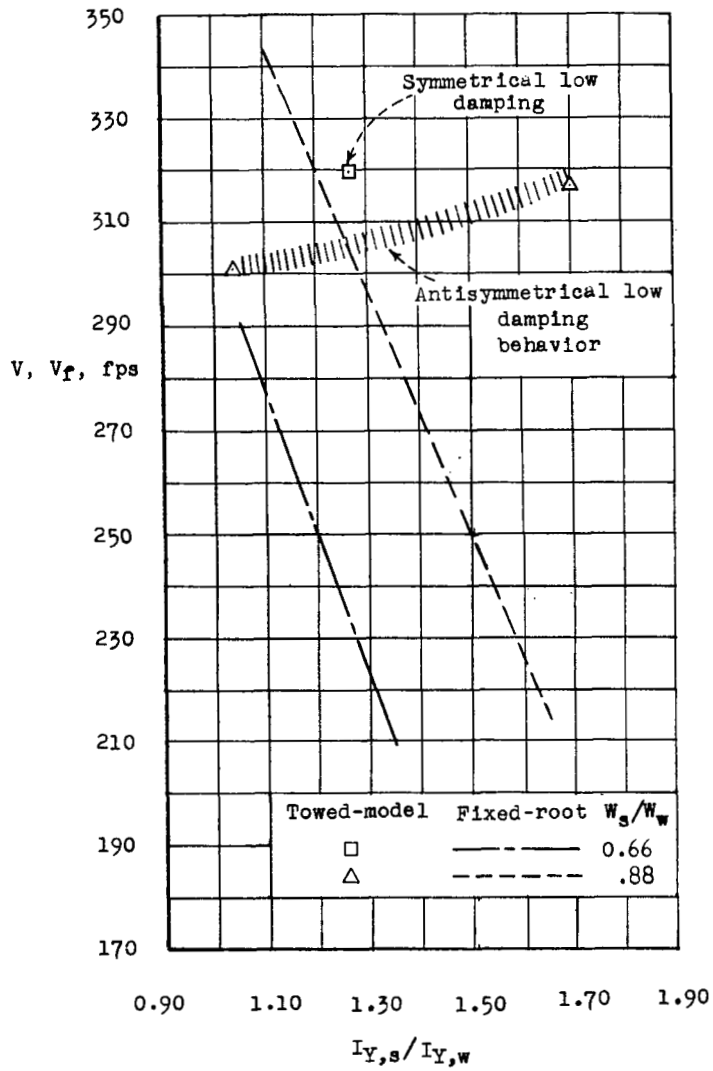
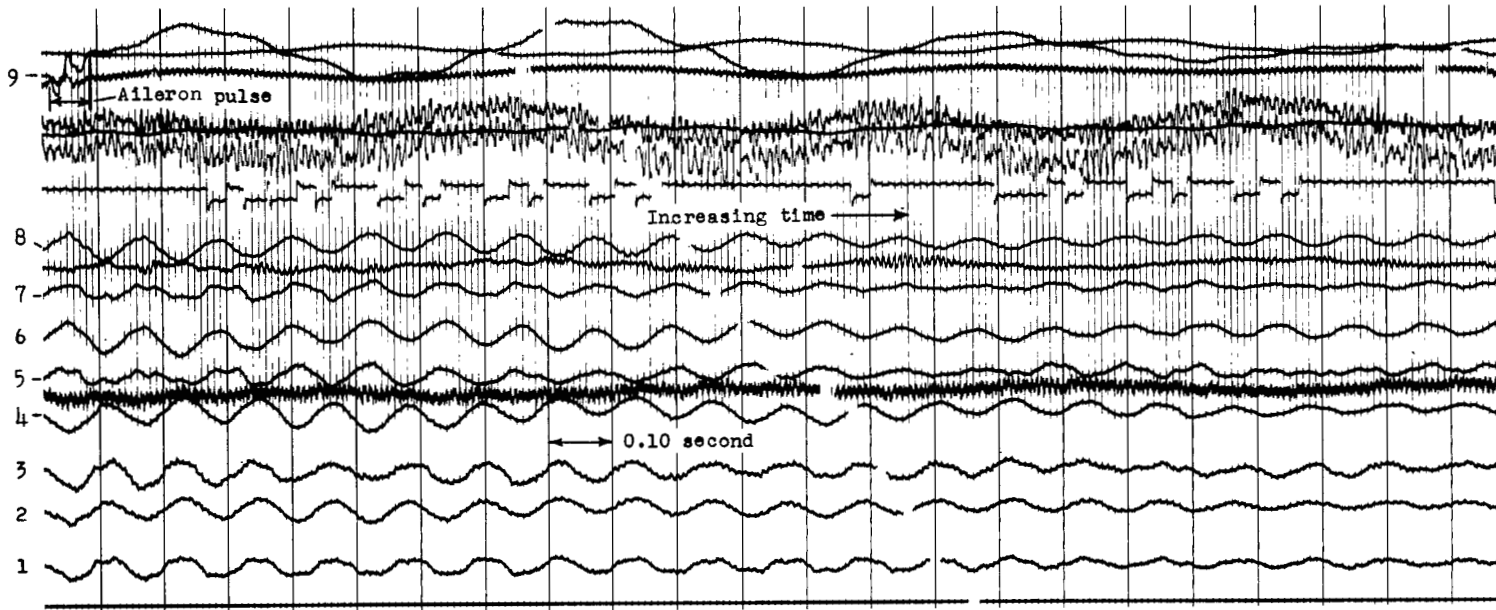


Figure 11.- Towed-model test results and comparison with the fixed-root flutter characteristics.



Trace	Item	Fraction semispan	Trace	Item	Fraction semispan
1	R. bending	0.50	5	L. bending	.66
2	R. torsion	.50	6	L. torsion	.66
3	R. bending	.66	7	L. bending	.50
4	R. torsion	.66	8	L. torsion	.50
			9	L. aileron deflection	

Figure 12.- Portion of oscillogram taken during a towed-model test showing the decay of wing motions following an aileron pulse near the maximum test airspeed for the 88-15-104 configuration. Directions of downward bending and torsion producing increased angles of attack are from bottom to top of figure.

NASA Technical Library



3 1176 01437 2339

